

An Improved Model for the Turbulent PBL

Y. CHENG, V. M. CANUTO,* AND A. M. HOWARD

NASA Goddard Institute for Space Studies, New York, New York

(Manuscript received 30 November 2000, in final form 26 September 2001)

ABSTRACT

Second-order turbulence models of the Mellor and Yamada type have been widely used to simulate the planetary boundary layer (PBL). It is, however, known that these models have several deficiencies. For example, assuming the production of the turbulent kinetic energy equals its dissipation, they all predict a critical Richardson number that is about four times smaller than the large eddy simulation (LES) data in stably stratified flows and are unable to distinguish the vertical and lateral components of the turbulent kinetic energy in neutral PBLs, and they predict a boundary layer height lower than expected.

In the present model, three new ingredients are employed: 1) an updated expression for the pressure–velocity correlation, 2) an updated expression for the pressure–temperature correlation, and 3) recent renormalization group (RNG) expressions for the different turbulence timescales, which yield

- 1) a critical Richardson number of order unity in the stably stratified PBL (at level 2 of the model),
- 2) different vertical and lateral components of the turbulent kinetic energy in the neutral PBL obtained without the use of the wall functions,
- 3) a greater PBL height,
- 4) closer comparisons with the Kansas data in the context of the Monin–Obukhov PBL similarity theory, in both stable and unstable PBLs, and
- 5) more realistic comparisons with the LES and laboratory data.

1. Introduction

Reynolds stress turbulence modeling began in the early 1940s (Chou 1940, 1945) and since then it has been developed by both physicists and engineers (e.g., Rotta 1951; Lumley and Khajeh-Nouri 1974; Launder et al. 1975; Pope 1975; Zeman and Lumley 1979; Speziale 1991; Shih and Shabbir 1992). The parameterizations of the turbulence closures have been formulated theoretically, verified experimentally (including comparison with the ever more reliable LES data), and applied to various engineering flows. In the geophysical applications, Mellor (1973), Mellor and Yamada (1974), and Mellor and Yamada (1982) pioneered the use of turbulence closure models to study the planetary boundary layer (PBL). The Mellor–Yamada (MY) model and its numerous variants have been more successful in the simulation of the PBL than many of the empirical models and have been widely used to describe the atmospheric PBL and the oceanic mixed layer. The MY mod-

els are, however, not without deficiencies. Comparison of MY model results with measured data and LES data show consistent discrepancies, and close examination indicates that the weakness of the model comes from three sources: 1) a crude parameterization for the pressure–velocity and the pressure–temperature correlations, 2) the use of a single “master” length scale (all the length scales corresponding to different processes are assumed to be proportional to a master scale), and 3) a downgradient approximation for the third-order turbulent moments. These three aspects can be handled as three independent components in the model development and each of them deserves a separate discussion. Along with many other efforts, the present authors tried to address items 2 and 3 elsewhere (Cheng and Canuto 1994; Canuto et al. 1994, 2001). The present paper concentrates on item 1, that is, how to improve the parameterization for the pressure correlations, thus generalizing the MY models and improving the comparison with both measured and LES data. The LES has been widely and successfully employed in the PBL (e.g., Moeng and Wyngaard 1986, 1989; Moeng and Sullivan 1994) and LES results have been regarded as experimental data, which are useful to guide and to test theoretical studies.

Let us look at deficiency 1 of the MY models and its variants (e.g., Galperin et al. 1988) more closely. First,

* Additional affiliation: Department of Applied Physics and Mathematics, Columbia University, New York, New York.

Corresponding author address: Dr. V. M. Canuto, NASA Goddard Institute for Space Studies, 2880 Broadway, New York, NY 10025.
E-mail: acvmc@giss.nasa.gov.

the level 2 (see section 5 for details) of these models predicts too low a critical Richardson (Ri_c) number (around 0.2), beyond which the turbulence ceases to exist, while both measurements and LES data (e.g., Webster 1964; Young 1975; Wang et al. 1996) indicate that the critical value is around unity. Second, when applied to the neutral boundary layer, assuming production equals dissipation, none of these models is capable of differentiating between the vertical and lateral components of the turbulent kinetic energy, $\frac{1}{2}w^2$ and $\frac{1}{2}v^2$; in fact, they yield identical expressions for the two, while experiments consistently show that the vertical component is much smaller than the lateral one (Table 1 of Mellor and Yamada 1982; Nieuwstadt 1985).

As we will show below, these deficiencies are associated with the oversimplification of the parameterizations of the pressure–velocity correlation Π_{ij}^θ and pressure–temperature correlation Π_i^θ , which will be corrected by adopting more complete expressions. Both Π_{ij}^θ and Π_i^θ have been shown to contain a slow (return-to-isotropy) part and a rapid part (Lauder et al. 1975; Lumley 1978). The rapid parts of both Π_{ij}^θ and Π_i^θ contain velocity terms related to the mean strain-rate tensor S_{ij} , and the vorticity tensor R_{ij} , as well as buoyancy terms related to the heat fluxes. In addition, the rapid part of Π_{ij}^θ also contains a term related to the temperature variance θ^2 . By contrast, MY models of Π_{ij}^θ include only the slow part and some of the rapid part (the term proportional to eS_{ij} , where e is the turbulent kinetic energy); for Π_i^θ , only the slow part is included. Since each of these missing terms represents a specific physical process, it seems appropriate and necessary to incorporate them in the model formulation, as we do in the present paper.

In sections 2, 3, and 4, we introduce the basic equations and the new turbulence closure. In section 5, we derive the new algebraic Reynolds stress and heat flux model for the PBL. The new model is presented in three different “levels” according to MY’s terminology. In section 6, a new value of the critical Richardson number is derived and discussed. Model constants are determined in section 7. In section 8, we compare the new model and the MY model with measured and LES data, where we can see that the new model matches the measured and LES data better than previous models. Conclusions are presented in section 9.

2. Mean field equations

To model a PBL, we need both mean and turbulent variables. The governing equations for mean fields are as follows:

1) mean velocity, U_i :

$$\frac{DU_i}{Dt} = -\frac{\partial}{\partial x_j} \tau_{ij} - g_i - \frac{1}{\rho} \frac{\partial P}{\partial x_i} - 2\epsilon_{ijk} \Omega_j U_k; \quad (1a)$$

2) mean potential temperature, Θ :

$$\frac{D\Theta}{Dt} = -\frac{\partial}{\partial x_j} h_j, \quad (1b)$$

where

$$\frac{D}{Dt} \equiv \frac{\partial}{\partial t} + U_j \frac{\partial}{\partial x_j}, \quad \tau_{ij} \equiv \overline{u_i u_j}, \quad h_i \equiv \overline{u_i \theta}. \quad (1c)$$

Here u_i is the i th component of the turbulent velocity fluctuation, $g_i = (0, 0, g)$ is the gravitational acceleration, P is the mean pressure, ρ is the mean density, Ω_j is the rotation of the earth, τ_{ij} is the Reynolds stress, and h_i is the heat flux.

In the PBL, several approximations can be made to the equations for the mean wind and temperature. In Eq. (1a), the horizontal pressure gradient can be expressed in terms of the mean geostrophic wind components U_g and V_g as follows:

$$\frac{1}{\rho} \left(\frac{\partial P}{\partial x}, \frac{\partial P}{\partial y} \right) = f_c (V_g, -U_g) \quad (1d)$$

and the rotation term can be approximated as

$$-2\epsilon_{ijk} \Omega_j U_k = f_c \epsilon_{ij3} U_j, \quad (1e)$$

where x , y , and z are the eastward, northward, and vertical directions, respectively, $f_c = 2\Omega \sin\phi$ is the Coriolis parameter with Ω the angular velocity of the earth and ϕ the latitude. In Eq. (1b), the horizontal temperature gradient can be approximated with the thermal wind relation,

$$\left(\frac{\partial \Theta}{\partial x}, \frac{\partial \Theta}{\partial y} \right) = \frac{f_c}{g\alpha} \left(\frac{\partial V_g}{\partial z}, -\frac{\partial U_g}{\partial z} \right), \quad (1f)$$

where α is the volume expansion coefficient.

The equations for the eastward and northward horizontal mean wind components U and V and for the mean potential temperature Θ in the PBL can then be written as

$$\frac{\partial U}{\partial t} = f_c (V - V_g) - \frac{\partial \overline{uw}}{\partial z} \quad (1g)$$

$$\frac{\partial V}{\partial t} = -f_c (U - U_g) - \frac{\partial \overline{vw}}{\partial z} \quad (1h)$$

$$\frac{\partial \Theta}{\partial t} = -\frac{\partial}{\partial z} \overline{w\theta} + \frac{f_c}{g\alpha} \left(V \frac{\partial U_g}{\partial z} - U \frac{\partial V_g}{\partial z} \right) - W \frac{\partial \Theta}{\partial z}. \quad (1i)$$

3. Turbulence equations

1) Reynolds stresses, τ_{ij} :

$$\begin{aligned} \frac{D}{Dt} \tau_{ij} + D_{ij} = & - \left(\tau_{ik} \frac{\partial U_j}{\partial x_k} + \tau_{jk} \frac{\partial U_i}{\partial x_k} \right) + \beta_i h_j \\ & + \beta_j h_i - \Pi_{ij} - \epsilon_{ij}, \end{aligned} \quad (2a)$$

where

$$\Pi_{ij} \equiv \overline{u_i \frac{\partial p}{\partial x_j}} + \overline{u_j \frac{\partial p}{\partial x_i}} - \frac{2}{3} \delta_{ij} \frac{\partial}{\partial x_k} \overline{p u_k} \quad (2b)$$

$$\epsilon_{ij} \equiv 2\nu \frac{\partial u_i}{\partial x_k} \frac{\partial u_j}{\partial x_k} = \frac{2}{3} \delta_{ij} \epsilon, \quad \beta_i \equiv \alpha g_i \quad (2c)$$

$$D_{ij} \equiv \frac{\partial}{\partial x_k} \left(\overline{u_i u_j u_k} + \frac{2}{3} \delta_{ij} \overline{p u_k} \right). \quad (2d)$$

Here, Π_{ij} is the pressure–velocity correlation tensor, ν is the molecular viscosity, ϵ is the dissipation rate of the turbulent kinetic energy e , and D_{ij} is the diffusion term.

2) Turbulent kinetic energy e :

$$e = \frac{1}{2} q^2, \quad q^2 \equiv \overline{u_i u_i} \quad (2e)$$

$$\frac{De}{Dt} + \frac{1}{2} D_{ii} = -\tau_{ij} \frac{\partial U_i}{\partial x_j} + \beta_i h_i - \epsilon. \quad (2f)$$

3) Heat flux, h_i :

$$\frac{D}{Dt} h_i + D_i^h = -h_j \frac{\partial U_i}{\partial x_j} - \tau_{ij} \frac{\partial \Theta}{\partial x_j} + \beta_i \overline{\theta^2} - \Pi_i^\theta, \quad (3a)$$

where

$$\Pi_i^\theta \equiv \overline{\theta \frac{\partial p}{\partial x_i}}, \quad D_i^h = \frac{\partial}{\partial x_j} \overline{u_i u_j \theta}, \quad (3b)$$

where Π_i^θ is the pressure–temperature correlation, and D_i^h is the diffusion of the heat flux h_i .

4) Temperature variance, θ^2 :

$$\frac{D}{Dt} \overline{\theta^2} + D_\theta = -2h_i \frac{\partial \Theta}{\partial x_i} - 2\epsilon_\theta, \quad (4a)$$

where

$$\epsilon_\theta \equiv \chi \left(\frac{\partial \theta}{\partial x_j} \right)^2, \quad D_\theta = \frac{\partial}{\partial x_i} \overline{u_i \theta^2}, \quad (4b)$$

where χ is the molecular conductivity, D_θ is the diffusion of the temperature variance, and ϵ_θ is the temperature variance dissipation rate.

In the present study, terms containing the molecular viscosity ν and molecular conductivity χ have been neglected, except for ϵ_{ij} and ϵ_θ . In addition, in the second-moment equations, rotation has also been neglected. The modeling of the third-order moments exceeds the scope of the present paper, but the interested readers may refer to recent work on the subject (Canuto et al. 1994, 2001). As already stated, in this paper we concentrate on the closure parameterization of the correlations Π_{ij} and Π_i^θ , which will be shown to improve the PBL model results.

4. Turbulence closure

a. ϵ and ϵ_θ

Equations (2f) and (4a) contain the two turbulence variables,

$$\epsilon, \epsilon_\theta, \quad (5a)$$

which represent the rates of dissipation of e and $\overline{\theta^2}$, and are contributed mostly by small scales with small energy content but large vorticity. On the other hand, e and $\overline{\theta^2}$ are contributed mostly by the large scales with most of the energy and little vorticity.

Even though exact dynamic equations for ϵ and ϵ_θ can and have been derived, they are of little practical use since most of the terms are difficult to interpret physically, and thus difficult to represent. A phenomenological equation for ϵ has been proposed long ago and in the case of pure shear flows, it has been used quite extensively in spite of containing two adjustable coefficients. When buoyancy is included, the number of unknown coefficients increases and it is difficult to calibrate them so as to assure any type of generality. Due to these difficulties, it is customary to use an alternative approach, namely one employs the basic relation (Batchelor 1971)

$$\epsilon = \frac{e^{3/2}}{\Lambda}, \quad (5b)$$

where Λ is the dissipation length scale. Rewriting (5b) in terms of Λ and τ defined as

$$\tau = \frac{2e}{\epsilon} \quad (5c)$$

one has

$$\epsilon = \frac{8\Lambda^2}{\tau^3}. \quad (5d)$$

In section 4b we will discuss how τ is determined, thus the determination of ϵ reduces to the modeling of Λ , a variable that has been extensively studied in the past. Here, we employ the Blackadar–Deardorff (Blackadar 1962; Deardorff 1980) model whereby

$$l = \frac{2^{3/2} \Lambda}{B_1} = \begin{cases} l_1: & \frac{\partial \Theta}{\partial z} \leq 0 \\ \min\left(l_1, 0.53 \frac{q}{N}\right): & \frac{\partial \Theta}{\partial z} > 0 \end{cases}$$

$$l_1 = \frac{\kappa z l_0}{l_0 + \kappa z}, \quad l_0 = 0.1 \frac{\int_0^\infty z q \, dz}{\int_0^\infty q \, dz}$$

$$N^2 \equiv g \alpha \frac{\partial \Theta}{\partial z}, \quad (5e)$$

where B_1 is a constant, which will be determined in section 7. Equation (5e) has been used in the PBL context by many authors (e.g., André et al. 1978; Hassid and Galperin 1983; Galperin et al. 1988).

The differential equation for ϵ_θ is even more difficult to calibrate than the ϵ equation and also too complicated to use. We use instead the parameterization

$$\epsilon_\theta = \frac{\overline{\theta^2}}{\tau_\theta} \quad (5f)$$

and we will determine the timescale τ_θ in section 7.

b. e and $\overline{\theta^2}$

The dynamic equations for e and $\overline{\theta^2}$ are given by Eqs. (2f) and (4a). In the so-called level-3 model these two differential equations are solved. In the level-2.5 model, the $\overline{\theta^2}$ equation is reduced to an algebraic equation by neglecting the storage, advection, and diffusion terms. In the level-2 model one similarly simplifies the e equation by assuming that production of e equals its dissipation:

$$P_b + P_s = \epsilon, \quad (5g)$$

where $P_{s,b}$ represent the production terms due to shear and buoyancy, respectively. Each production term is proportional to the gradient of the mean variable in question times a turbulent diffusivity K [e.g., see Eqs. (16a,b)]. In terms of the basic variables e and ϵ , K has the dependence

$$K \sim ul \sim e^{1/2} l \sim \frac{e^2}{\epsilon} \quad (5h)$$

and thus the solution of (5g) does not yield e or ϵ separately but only their ratio τ ,

$$\tau N = f(\text{Ri}). \quad (5i)$$

The function $f(\text{Ri})$ is thus uniquely determined by (5g) as a function of Ri and, as expected, τ grows with Ri indicating that for a fixed shear, the larger the stratification, the weaker is the turbulence and the longer is the timescale τ . In the limit $\tau \rightarrow \infty$, one may consider the flow to have become almost laminar, namely the eddies have an infinite lifetime, they no longer break up, thus no cascade process exists. On the other hand, for small Ri , the stratification is weak, turbulence dominates, and the eddies tend to break up quite easily due to the strong nonlinear interactions. In other words, $\tau N \gg 1$ corresponds to weak turbulence while $\tau N \ll 1$ corresponds to strong turbulence.

c. Pressure correlations

The pressure correlation terms Π_{ij} and Π_i^θ in Eqs. (2b) and (3b) contain three distinct contributions due to 1) turbulence self-interactions (the return-to-isotropy or slow part), 2) mean shear–turbulence interactions (a rap-

id part), and 3) buoyancy–turbulence interactions (also a rapid part). The most complete models for Π_{ij} and Π_i^θ are given by (Launder et al. 1975; Zeman and Lumley 1979):

$$\begin{aligned} \Pi_{ij} &= \Pi_{ij}^{(1)} + \Pi_{ij}^{(2)} + \Pi_{ij}^{(3)}, \\ \Pi_i^\theta &= \Pi_i^{\theta(1)} + \Pi_i^{\theta(2)} + \Pi_i^{\theta(3)}, \end{aligned} \quad (6a)$$

where

$$\begin{aligned} \Pi_{ij}^{(1)} &= 2\tau_{pv}^{-1} b_{ij} \\ \Pi_{ij}^{(2)} &= -\frac{4}{5} e S_{ij} - \alpha_1 \Sigma_{ij} - \alpha_2 Z_{ij} \\ \Pi_{ij}^{(3)} &= (1 - \beta_5) B_{ij} \end{aligned} \quad (6b)$$

$$\begin{aligned} \Pi_i^{\theta(1)} &= \tau_{p\theta}^{-1} h_i & \Pi_i^{\theta(2)} &= -\frac{3}{4} \alpha_3 \left(S_{ij} + \frac{5}{3} R_{ij} \right) h_j \\ \Pi_i^{\theta(3)} &= \gamma_1 \beta_i \overline{\theta^2}, \end{aligned} \quad (6c)$$

where b_{ij} is the traceless Reynolds stress tensor defined as follows:

$$b_{ij} = \overline{u_i u_j} - \frac{2e}{3} \delta_{ij}. \quad (6d)$$

The other tensors are defined as follows:

$$\begin{aligned} S_{ij} &= \frac{1}{2} \left(\frac{\partial U_i}{\partial x_j} + \frac{\partial U_j}{\partial x_i} \right), & R_{ij} &= \frac{1}{2} \left(\frac{\partial U_i}{\partial x_j} - \frac{\partial U_j}{\partial x_i} \right) \\ \Sigma_{ij} &= b_{ik} S_{kj} + S_{ik} b_{kj} - \frac{2}{3} \delta_{ij} b_{km} S_{mk}, \\ Z_{ij} &= R_{ik} b_{kj} - b_{ik} R_{kj} \\ B_{ij} &= \beta_i h_j + \beta_j h_i - \frac{2}{3} \delta_{ij} \beta_k h_k, \end{aligned} \quad (6e)$$

where S_{ij} and R_{ij} are shear and vorticity, respectively.

In most past second-order turbulence models for the PBL, the pressure correlations terms were parameterized much less completely than in (6a)–(6c). For Π_{ij} , the MY (1982; Mellor 1973) and Kantha and Clayson (1994) models only consider:

$$\Pi_{ij}^{(1)} = 2\tau_{pv}^{-1} b_{ij}, \quad \Pi_{ij}^{(2)} \sim -e S_{ij}, \quad \Pi_{ij}^{(3)} = 0; \quad (7a)$$

for Π_i^θ , the MY model contains only the terms

$$\Pi_i^{\theta(1)} = \tau_{p\theta}^{-1} h_i, \quad \Pi_i^{\theta(2)} = \Pi_i^{\theta(3)} = 0. \quad (7b)$$

Namely, the MY model includes only the slow terms and one single rapid term (the first term in the expression of $\Pi_{ij}^{(2)}$); most of the rapid terms are neglected, and no buoyancy effects are included. The models by Kantha and Clayson (1994) and D'Alessio et al. (1998) improve the parameterization for Π_i^θ , but the $\Pi_i^{\theta(2)}$ term is still missing,

$$\Pi_i^{\theta(1)} = \tau_{p\theta}^{-1} h_i, \quad \Pi_i^{\theta(2)} = 0, \quad \Pi_i^{\theta(3)} = \gamma_1 \beta_i \overline{\theta^2}. \quad (7c)$$

More complete parameterizations of both Π_{ij} and Π_i^θ

were used by Gambo (1978), Yamada (1985), and Nak-anishi (2001), but α_1 and α_2 were either taken to be identical or set to zero in Eq. (6b), and S_{ij} and R_{ij} were set to have the same coefficient in Eq. (6c).

In section 5, we will derive new expressions for the stability functions (S_M and S_H) using the more complete pressure correlations. In the following sections, we will show that previous parameterizations of the pressure correlations are at the root of some model deficiencies, for example, the inability to match the data in the neutral boundary layer as well as in the stably and unstably stratified flows.

5. Algebraic Reynolds stress and heat flux models

a. Algebraic equations for the second moments

Combining (2a) and (2f) and using (5c), we obtain the equation for b_{ij} , defined in Eq. (6d):

$$\frac{D}{Dt}b_{ij} + D_{ij} = -\frac{4}{3}eS_{ij} - \Sigma_{ij} - Z_{ij} + B_{ij} - \Pi_{ij}, \quad (8a)$$

where

$$D_{ij} \equiv \frac{\partial}{\partial x_k} \overline{\left(u_i u_j - \frac{1}{3} u_i u_l \delta_{ij} \right) u_k}. \quad (8b)$$

Assuming that the left side of (8a) can be neglected and employing (6b) for the pressure-velocity correlation Π_{ij} , one obtains the following algebraic equation for b_{ij}

$$b_{ij} = -\lambda_1 e \tau S_{ij} - \lambda_2 \tau \Sigma_{ij} - \lambda_3 \tau Z_{ij} + \lambda_4 \tau B_{ij}, \quad (9a)$$

where

$$\begin{aligned} \lambda &= \frac{\tau_{pv}}{\tau}, & \lambda_1 &= \frac{4}{15} \lambda, & \lambda_2 &= \frac{1}{2} (1 - \alpha_1) \lambda \\ \lambda_3 &= \frac{1}{2} (1 - \alpha_2) \lambda, & \lambda_4 &= \frac{1}{2} \beta_5 \lambda. \end{aligned} \quad (9b)$$

These model constants will be given in section 7. Similarly, in the prognostic equation (3a) for the heat flux h_i , if one neglects the left side and use is made of (6c) for Π_i^θ , one obtains the algebraic equation for h_i at level 3:

$$A_{ij} h_j = -\tau \left(b_{ij} + \frac{2e}{3} \delta_{ij} \right) \frac{\partial \Theta}{\partial x_j} + \lambda_0 \tau \beta_i \overline{\theta^2}, \quad (10a)$$

where

$$A_{ij} = \lambda_5 \delta_{ij} + \lambda_6 \tau S_{ij} + \lambda_7 \tau R_{ij} \quad (10b)$$

$$\begin{aligned} \lambda_0 &= 1 - \gamma_1, & \lambda_5 &= \frac{\tau}{\tau_{p\theta}}, & \lambda_6 &= 1 - \frac{3}{4} \alpha_3, \\ \lambda_7 &= 1 - \frac{5}{4} \alpha_3. \end{aligned} \quad (10c)$$

At levels 2.5 and 2, we further simplify the problem by neglecting the left side in the prognostic equation

for $\overline{\theta^2}$, Eq. (4a), to obtain the algebraic equation

$$\overline{\theta^2} = -\tau_\theta h_i \frac{\partial \Theta}{\partial x_i}. \quad (11)$$

Substituting (11) into (10a), we obtain the algebraic equation for h_i at levels 2.5–2:

$$A'_{ij} h_j = -\tau \left(b_{ij} + \frac{2e}{3} \delta_{ij} \right) \frac{\partial \Theta}{\partial x_j}, \quad (12a)$$

where

$$A'_{ij} = \lambda_5 \delta_{ij} + \lambda_6 \tau S_{ij} + \lambda_7 \tau R_{ij} + \lambda_8 \tau^2 \beta_i \frac{\partial \Theta}{\partial x_j} \quad (12b)$$

and where

$$\lambda_8 = (1 - \gamma_1) \frac{\tau_\theta}{\tau}. \quad (12c)$$

In the following subsections, we will present a hierarchy of turbulence models for the PBL.

b. Level-3 model

Since the level-2.5 and level-2 models catch the main features of the second-order closure models and are easy to use, they have become the most popular second-order closure models in the PBL community. We will concentrate on them in the sections below. Yet, the level-3 model has its own strength in that it produces countergradient heat fluxes, a phenomenon observed in the upper part of the convective PBL. In the appendix we will present the details of the level-3 model for completeness and for future reference.

c. Level-2.5 model

In the level-2.5 model, the turbulent kinetic energy e is solved from its prognostic equation (2f):

$$\begin{aligned} \frac{\partial e}{\partial t} &= -\frac{\partial}{\partial z} \frac{1}{2} \overline{u^2 w + v^2 w + w^3} - \frac{\partial U}{\partial z} \overline{uw} \\ &\quad - \frac{\partial V}{\partial z} \overline{vw} + g \alpha \overline{w\theta} - \epsilon. \end{aligned} \quad (13)$$

The equation for the temperature variance $\overline{\theta^2}$ is

$$\overline{\theta^2} = -\tau_\theta \overline{w\theta} \frac{\partial \Theta}{\partial z}. \quad (14)$$

From the algebraic equations for $\overline{u_i u_j}$ and $\overline{u_i \theta}$, Eqs. (9a) and (12a), we obtain:

$$\overline{u^2} = \frac{1}{3}q^2 - \frac{\tau}{3}\left[(\lambda_2 + 3\lambda_3)\frac{\partial U}{\partial z}\overline{uw} - 2\lambda_2\frac{\partial V}{\partial z}\overline{vw} + 2\lambda_4g\alpha\overline{w\theta}\right] \tag{15a}$$

$$\overline{v^2} = \frac{1}{3}q^2 - \frac{\tau}{3}\left[(\lambda_2 + 3\lambda_3)\frac{\partial V}{\partial z}\overline{vw} - 2\lambda_2\frac{\partial U}{\partial z}\overline{uw} + 2\lambda_4g\alpha\overline{w\theta}\right] \tag{15b}$$

$$\overline{w^2} = \frac{1}{3}q^2 + \frac{\tau}{3}\left[(3\lambda_3 - \lambda_2)\left(\frac{\partial U}{\partial z}\overline{uw} + \frac{\partial V}{\partial z}\overline{vw}\right) + 4\lambda_4g\alpha\overline{w\theta}\right] \tag{15c}$$

$$\overline{uw} = -(\lambda_2 + \lambda_3)\frac{\tau}{2}\left(\frac{\partial V}{\partial z}\overline{uw} + \frac{\partial U}{\partial z}\overline{vw}\right) \tag{15d}$$

$$\overline{uw} = -\frac{\tau}{2}\frac{\partial U}{\partial z}\left[\frac{1}{2}\left(\lambda_1 - \frac{4}{3}\lambda_2\right)q^2 + (\lambda_2 - \lambda_3)\overline{u^2} + (\lambda_2 + \lambda_3)\overline{w^2}\right] - (\lambda_2 - \lambda_3)\frac{\tau}{2}\frac{\partial V}{\partial z}\overline{uw} + \lambda_4\tau g\alpha\overline{u\theta} \tag{15e}$$

$$\overline{vw} = -\frac{\tau}{2}\frac{\partial V}{\partial z}\left[\frac{1}{2}\left(\lambda_1 - \frac{4}{3}\lambda_2\right)q^2 + (\lambda_2 - \lambda_3)\overline{v^2} + (\lambda_2 + \lambda_3)\overline{w^2}\right] - (\lambda_2 - \lambda_3)\frac{\tau}{2}\frac{\partial U}{\partial z}\overline{vw} + \lambda_4\tau g\alpha\overline{v\theta} \tag{15f}$$

$$\overline{u\theta} = -\lambda_5^{-1}\tau\left[\frac{\partial\Theta}{\partial z}\overline{uw} + \frac{1}{2}(\lambda_6 + \lambda_7)\frac{\partial U}{\partial z}\overline{w\theta}\right] \tag{15g}$$

$$\overline{v\theta} = -\lambda_5^{-1}\tau\left[\frac{\partial\Theta}{\partial z}\overline{vw} + \frac{1}{2}(\lambda_6 + \lambda_7)\frac{\partial V}{\partial z}\overline{w\theta}\right] \tag{15h}$$

$$\overline{w\theta} = -\lambda_5^{-1}\tau\left[\frac{\partial\Theta}{\partial z}\overline{w^2} + \frac{1}{2}(\lambda_6 - \lambda_7)\left(\frac{\partial U}{\partial z}\overline{u\theta} + \frac{\partial V}{\partial z}\overline{v\theta}\right)\right] \times \left[1 + \lambda_5^{-1}\lambda_8g\alpha\tau^2\frac{\partial\Theta}{\partial z}\right]^{-1} \tag{15i}$$

$$(\overline{uw}, \overline{vw}) = -K_M\left(\frac{\partial U}{\partial z}, \frac{\partial V}{\partial z}\right) \tag{16a}$$

$$\overline{w\theta} = -K_H\frac{\partial\Theta}{\partial z} \tag{16b}$$

$$K_M = e\tau S_M, \quad K_H = e\tau S_H \tag{16c}$$

$$S_M = \frac{1}{D}(s_0 + s_1G_H + s_2G_M) \tag{17a}$$

$$S_H = \frac{1}{D}(s_4 + s_5G_H + s_6G_M), \tag{17b}$$

where G_H and G_M are defined as

$$G_H \equiv (\tau N)^2, \quad G_M \equiv (\tau S)^2 \tag{18a}$$

$$N^2 \equiv g\alpha\frac{\partial\Theta}{\partial z}, \quad S^2 \equiv \left(\frac{\partial U}{\partial z}\right)^2 + \left(\frac{\partial V}{\partial z}\right)^2 \text{ and } \tag{18b}$$

$$D = 1 + d_1G_H + d_2G_M + d_3G_H^2 + d_4G_HG_M + d_5G_M^2 \tag{18c}$$

$$d_1 = \lambda_5^{-1}\left(\frac{7}{3}\lambda_4 + \lambda_8\right)$$

$$d_2 = \left(\lambda_3^2 - \frac{1}{3}\lambda_2^2\right) - \frac{1}{4}\lambda_5^{-2}(\lambda_6^2 - \lambda_7^2),$$

$$d_3 = \frac{1}{3}\lambda_4\lambda_5^{-2}(4\lambda_4 + 3\lambda_8)$$

$$d_4 = \frac{1}{3}\lambda_4\lambda_5^{-2}[\lambda_2\lambda_6 - 3\lambda_3\lambda_7 - \lambda_5(\lambda_2^2 - \lambda_3^2)]$$

$$+ \lambda_5^{-1}\lambda_8\left(\lambda_3^2 - \frac{1}{3}\lambda_2^2\right)$$

$$d_5 = -\frac{1}{4}\lambda_5^{-2}\left(\lambda_3^2 - \frac{1}{3}\lambda_2^2\right)(\lambda_6^2 - \lambda_7^2), \quad s_0 = \frac{1}{2}\lambda_1$$

$$s_1 = -\frac{1}{3}\lambda_4\lambda_5^{-2}(\lambda_6 + \lambda_7) + \frac{2}{3}\lambda_4\lambda_5^{-1}\left(\lambda_1 - \frac{1}{3}\lambda_2 - \lambda_3\right) + \frac{1}{2}\lambda_1\lambda_5^{-1}\lambda_8$$

$$s_2 = -\frac{1}{8}\lambda_1\lambda_5^{-2}(\lambda_6^2 - \lambda_7^2), \quad s_4 = \frac{2}{3}\lambda_5^{-1},$$

$$s_5 = \frac{2}{3}\lambda_4\lambda_5^{-2}$$

$$s_6 = \frac{2}{3}\lambda_5^{-1}\left(\lambda_3^2 - \frac{1}{3}\lambda_2^2\right) - \frac{1}{2}\lambda_1\lambda_5^{-1}\left(\lambda_3 - \frac{1}{3}\lambda_2\right)$$

$$+ \frac{1}{4}\lambda_1\lambda_5^{-2}(\lambda_6 - \lambda_7). \tag{18d}$$

Equations (15a)–(15i) can be solved using symbolic algebra. The results are

In the above, the definitions of the stability functions S_M and S_H as well as the dimensionless gradients G_M and G_H are different than the corresponding definitions in the MY model. The transformation between the notations is straightforward:

$$S_M = 2B_1^{-1}S_M(\text{MY}), \quad S_H = 2B_1^{-1}S_H(\text{MY}) \quad (19a)$$

$$G_M = B_1^2G_M(\text{MY}), \quad G_H = -B_1^2G_H(\text{MY}). \quad (19b)$$

In section 8 we will show that the MY model is a special case of the present model, and that the coefficients s_2 and d_5 are both nonzero in the new model and both zero in the MY model. Since s_2 appears in the expression for S_M via Eq. (17a) and d_5 appears in the expressions for both S_M and S_H via Eq. (18c), a “structural symmetry” can be seen in the new model while not in the MY model. By “structural symmetry,” we mean that: every G_H factor has a G_M counterpart, and both G_H and G_M enter with the same power. In the MY model, the term s_2G_M in (17a) and the term $d_5G_M^2$ in (18c) are missing.

d. Realizability conditions for level-2.5 model

Realizability requirements are common to second-order closure models. For the present 2.5-level model, the two variables G_M and G_H must be limited to certain domains outside of which the model may produce unphysical results since some underlying assumptions (e.g., that departure from isotropy be small) may no longer be valid.

Let us first consider the limitation on buoyancy. Here G_H may be negative (unstable), zero (neutral), or positive (stable). Assuming that production equals dissipation for the turbulence kinetic energy e [see Eq. (22) below], and taking the limit $G_M \rightarrow 0$ and noticing that G_M is always nonnegative, we have

$$S_H(0, G_H)G_H + 2 \geq 0. \quad (20a)$$

Substituting Eq. (17b) into Eq. (20a) yields the relation

$$G_H \geq \frac{-(s_4 + 2d_1) + [(s_4 + 2d_1)^2 - 8(s_5 + 2d_3)]^{1/2}}{2(s_5 + 2d_3)}. \quad (20b)$$

For the model constants used here (see section 7), this minimum value of G_H is -10.8 ; the negative value indicates that it occurs in the unstable region.

Next, we examine the limitation on the shear number. Following Hassid and Galperin (1983), who argue that an increase of shear should not result in a decrease of the normalized momentum flux, we apply the following condition,

$$\frac{d}{dG_M} \left[\frac{(\overline{uW}^2 + \overline{vW}^2)^{1/2}}{e} \right] \geq 0. \quad (21a)$$

Using Eqs. (16)–(18), Eq. (21a) can be reduced to a cubic inequality in G_M ,

$$\begin{aligned} & s_2d_5G_M^3 + [(3s_1d_5 - s_2d_4)G_H + 3s_0d_5 - s_2d_2]G_M^2 \\ & + [(s_1d_4 - 3s_2d_3)G_H^2 + (s_1d_2 + s_0d_4 - 3s_2d_1)G_H \\ & - 3s_2 + s_0d_2]G_M \\ & - (s_0 + s_1G_H)(d_3G_H^2 + d_1G_H + 1) \\ & < 0. \end{aligned} \quad (21b)$$

Although Eq. (21b) can be solved exactly, one may use the following approximate expression based on the fact that the terms containing s_2 and d_5 are relatively small,

$$G_M \leq \frac{1 + d_1G_H + d_3G_H^2}{d_2 + d_4G_H} \equiv G_M^{\max}. \quad (21c)$$

e. Level-2 model

If we assume that production equals dissipation, the differential equation for e , Eq. (13), reduces to

$$S_M(G_M, G_H)G_M - S_H(G_M, G_H)G_H - 2 = 0, \quad (22)$$

which can be rewritten as an equation for G_M (or for G_H) that depends on only one parameter, the gradient Richardson number,

$$\text{Ri} = \frac{G_H}{G_M} = \frac{N^2}{S^2}. \quad (23a)$$

Equation (22) then becomes

$$(c_1\text{Ri}^2 - c_2\text{Ri} + c_3)G_M^2 + (c_4\text{Ri} + c_5)G_M + 2 = 0, \quad (23b)$$

where

$$\begin{aligned} c_1 &= s_5 + 2d_3, & c_2 &= s_1 - s_6 - 2d_4, \\ c_3 &= -s_2 + 2d_5, & c_4 &= s_4 + 2d_1, \\ c_5 &= -s_0 + 2d_2. \end{aligned} \quad (23c)$$

It is important to check the consistency of (21c) with (23b). At level 2, the results are presented in Fig. 1, while the use of the MY model gives rise to the results presented in Fig. 2. It is apparent that in the present model, G_M is smaller than G_M^{\max} for all $\text{Ri} < \text{Ri}_c$ and thus the model is realizable. On the other hand, the MY G_M is larger than G_M^{\max} for $\text{Ri} \geq 0.064$, indicating that the MY model at level 2 is not compatible with Hassid and Galperin (1983)'s condition even for moderate Richardson numbers.

Substituting the G_M solved from (23b) into (17a,b) we can further plot the stability functions S_M and S_H as functions of Ri (Figs. 3 and 4).

6. Critical Richardson number

In the level-2 model, the critical Richardson number Ri_c , beyond which stable stratification effectively suppresses the turbulence, can be found by considering the

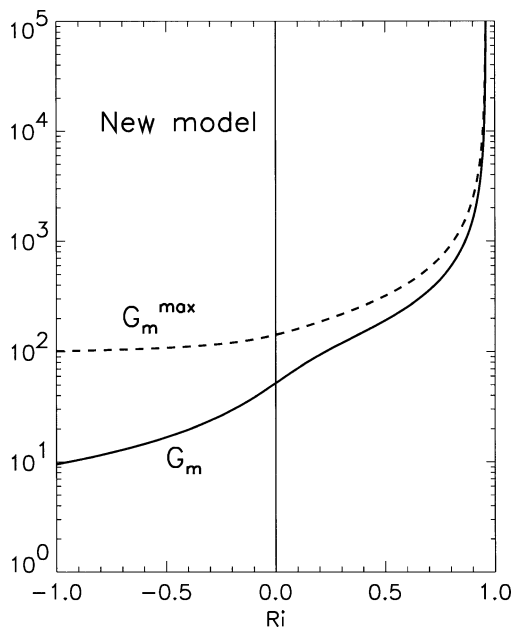


FIG. 1. Solid line: G_M as a function of the gradient Richardson number Ri , obtained from the present model at level 2, Eq. (23b); dashed line: G_M^{\max} as a function of Ri , obtained from Eq. (21c).

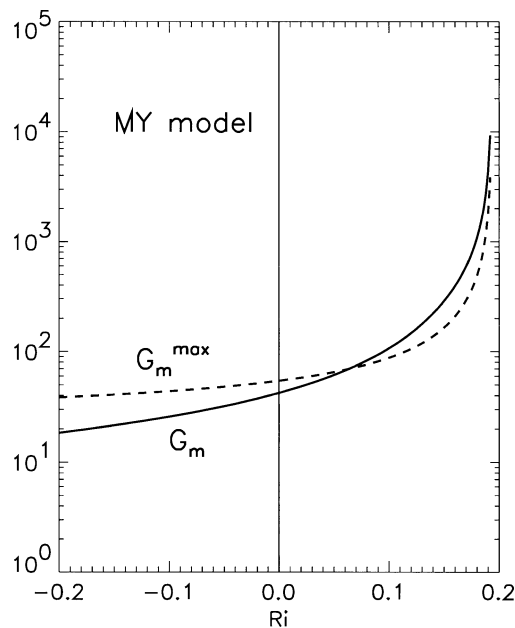


FIG. 2. Similar to Fig. 1 but for the MY model.

limit $e \rightarrow 0$, that is, $G_M \rightarrow \infty$. In this limit, Eq. (23b) is satisfied only if the coefficient of the quadratic term vanishes, which yields

$$Ri_c = \frac{c_2 + (c_2^2 - 4c_1c_3)^{1/2}}{2c_1}. \tag{24a}$$

Using the model constants determined in section 7, we obtain

$$Ri_c = 0.96. \tag{24b}$$

Although most previous second-order closure models give $Ri_c \sim 0.2$, there is a variety of data that are in favor of a Ri_c of order one. Early laboratory data by Taylor (as cited in Monin and Yaglom 1971) showed that turbulent exchange exists even when $Ri > 1$. Webster (1964) and Young (1975)'s laboratory measurements showed that mixing persists up to $Ri \sim 1$. In the oceanic PBL, Martin (1985) showed that $Ri \sim 1$ is needed to obtain the correct mixed layer depth at Papa and November stations. More recently, direct numerical simulation (DNS; Gerz et al. 1989) and LES (e.g., Wang et al. 1996; Kosovic and Curry 2000) show that turbulence exists up to $Ri \sim 1$. Historically, the criterion

$$Ri \geq \frac{1}{4} \tag{24c}$$

was established by Miles (1961) and Howard (1961) on the basis of linear stability analysis. However, when nonlinear interactions were included, Abarbanel et al. (1984) showed that the sufficient and necessary condition for stability is not (24c) but

$$Ri \geq 1, \tag{24d}$$

which is in agreement with our result (24b).

The numerical value of Ri_c given by (24b) is a consequence of the closure parameterizations and the values of the model constants via Eq. (24a). It is to be under-

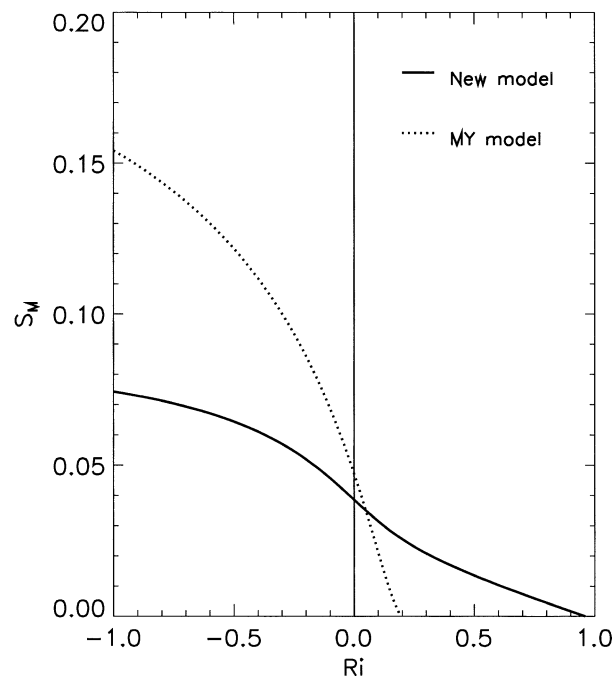


FIG. 3. The stability function S_M vs the gradient Richardson number Ri . The solid line represents the present model; the dotted line, the MY model. Note that the definitions of S_M and S_H and those in the MY model differ by a constant [see Eq. (19a)].

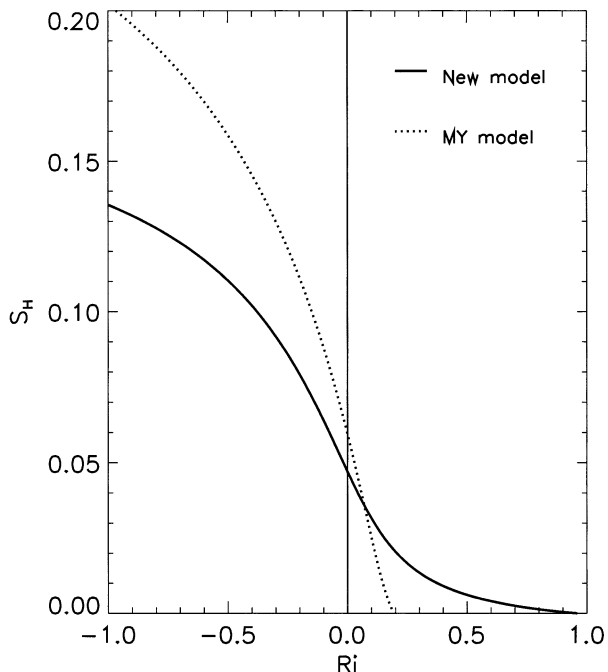


FIG. 4. Same as Fig. 3 but for the stability function S_H .

stood that different choices of the (often scattered) data underlying the model constants may lead to somewhat different values of Ri_c , and the best we can do is to choose the ones we believe are the best, guided by the theoretical, nonlinear analysis (Abarbanel et al. 1984) and numerous LES and laboratory results, which indicate that Ri_c should be of order unity (also see Strang and Fernando 2001). Therefore, the value 0.96 in (24b) should be regarded as a suggestion and is subject to some changes when more data become available.

7. Determination of model constants

A critical part in the determination of the closure parameters (defined in 9b, 10c, and 12c) is the turbulence timescale ratios τ_{pv} , $\tau_{p\theta}$ and τ_θ ; τ_{pv} , and $\tau_{p\theta}$ are the timescales that enter the first term in the pressure correlations (thus, the subscript p) for the velocity and temperature fields. In the phenomenological models these are known as the Rotta terms and their ratios to the dynamical timescale τ were considered adjustable parameters. In fact, many previous higher-order PBL models determine these timescale ratios empirically (for a summary, see Wichmann and Schaller 1986). In the present study we take a new approach: instead of treating these parameters as free, we employ the expressions from a recent theoretical turbulence model that was based in part on renormalization group (RNG) methods and whose predictions were tested on a variety of flows (Canuto and Dubovikov 1996a,b, 1997):

$$\frac{\tau_{pv}}{\tau} = \frac{2}{5}, \quad \frac{\tau}{\tau_{p\theta}} = 5(1 + \sigma_{i0}^{-1}), \quad \frac{\tau_\theta}{\tau} = \sigma_{i0}, \quad (25a)$$

where σ_{i0} is the turbulent Prandtl number in neutral flows and will be determined later on. Applying (25a) in (9b), (10c), and (12c) gives

$$\lambda = \frac{2}{5}, \quad \lambda_1 = 0.107, \quad \lambda_5 = 5(1 + \sigma_{i0}^{-1}),$$

$$\lambda_8 = (1 - \gamma_1)\sigma_{i0}, \quad \gamma_1 = \frac{1}{3}, \quad (25b)$$

where the value of γ_1 is also given by RNG.

To determine λ_2 , λ_3 , and λ_4 , we adopt the following expressions (Shih and Shabbir 1992; Canuto 1994):

$$\alpha_1 = 6\alpha_5, \quad \alpha_2 = \frac{2}{3}(2 - 7\alpha_5),$$

$$\alpha_5 = \frac{1}{10} \left(1 + \frac{4}{5}F^{1/2} \right), \quad F = 0.64,$$

$$\beta_5 = \frac{1}{2}, \quad (25c)$$

where the value of β_5 is given by RNG. Substituting (25a)–(25c) in (9b) yields

$$\lambda_2 = 0.0032, \quad \lambda_3 = 0.0864, \quad \lambda_4 = 0.1. \quad (25d)$$

We parameterize ϵ (the dissipation rate of e) as

$$\epsilon = \frac{q^3}{B_1 l}, \quad (26a)$$

which corresponds to

$$\tau = \frac{B_1 l}{q}, \quad (26b)$$

where the dissipation length scale $\ell \sim \kappa z$ as $z \sim 0$ and the constant B_1 is defined as $B_1 = q^3/u_*^3$, where u_* is the friction velocity, and the value of B_1 must be determined. In the neutral surface layer (taking the mean wind direction as the x direction), we derive from (15e) that B_1 is related to the values of λ_1 , λ_2 , and λ_3 :

$$B_1 = \left(\frac{1}{4}\lambda_1 - \lambda_3^2 + \frac{1}{3}\lambda_2^2 \right)^{-3/4} = 19.3, \quad (27)$$

where we have used the fact that $G_M \sim B_1^{4/3}$. This value of 19.3 for B_1 is different from the commonly used value of 16.6, which is determined in Mellor and Yamada (1982) by averaging several different data quoted in their Table 1. When different and/or new data are used in the averaging process, a new value of B_1 may be obtained. For example, Enger (1986) uses $B_1 = 27$ derived from Kansas spectra (Kaimal et al. 1972) and other laboratory data. A value of 27.4 was obtained for B_1 by Nieuwstadt (1985) and by Andr n and Moeng (1993), a value of 22.6 was used by Therry and Lacarr re (1983) and a value of 24 is used by Nakanishi (2001). Instead of trying to determine B_1 directly from the scattered data, we look into how the value of B_1 relates to the values of λ_1 , λ_2 , and λ_3 [Eq. (27)]. The value of λ_1 is

determined from the renormalization group theory presented in Canuto and Dubovikov (1996a,b; 1997). The values of λ_2 and λ_3 are from theoretical formulations that are shown to be consistent with measured data (Shih and Shabbir 1992; Canuto 1994). The value 19.3 for B_1 may be considered a compromise between the MY value (16.6) and the subsequent larger values.

To determine the values of λ_6 , λ_7 , and σ_{t0} , we need some auxiliary relations. First, from (15g), (15i), an expression for the ratio of the vertical and longitudinal heat fluxes can be derived,

$$-\frac{\overline{w\theta}}{u\theta} = \lambda_5 G_M^{-1/2} \left[\sigma_t + \frac{1}{2}(\lambda_6 + \lambda_7) \right]^{-1}, \quad (28a)$$

where $\sigma_t \equiv S_M/S_H$ is the turbulent Prandtl number. Webster's (1964) experimental data show that this ratio approaches unity as $Ri \sim 0$,

$$\lambda_5 B_1^{-2/3} \left[\sigma_{t0} + \frac{1}{2}(\lambda_6 + \lambda_7) \right]^{-1} = 1. \quad (28b)$$

Second, in a near-neutral surface layer, from (15g), (15i), we obtain

$$\lambda_5^2 - \frac{1}{3} B_1^{4/3} (1 + \lambda_2 - 3\lambda_3) \sigma_{t0} \lambda_5 - \frac{1}{4} B_1^{4/3} (\lambda_6 - \lambda_7) (2\sigma_{t0} + \lambda_6 + \lambda_7) = 0. \quad (28c)$$

Using (10c), (28b), and (28c), we obtain,

$$\alpha_3 = \frac{4}{5} + \frac{4}{5} \sigma_{t0} \left[1 - \frac{1}{3} B_1^{2/3} (1 + \lambda_2 - 3\lambda_3) \right] \quad (28d)$$

and λ_6 and λ_7 can be obtained using (28d) in (10c). We still need to determine a value for σ_{t0} in a consistent manner. From the third expression of (25b) and (28b)–(28d), σ_{t0} is found to be related to B_1 , λ_2 and λ_3 as follows:

$$\sigma_{t0} = \frac{75 - 3B_1^{2/3} + 3^{1/2}[1875 + 150B_1^{2/3} + (403 + 400\lambda_2 - 1200\lambda_3)B_1^{4/3}]^{1/2}}{2B_1^{2/3}[3 + 4B_1^{2/3}(1 + \lambda_2 - 3\lambda_3)]} = 0.82. \quad (29a)$$

So it follows that:

$$\begin{aligned} \lambda_5 &= 11.04, & \lambda_6 &= 0.786, & \lambda_7 &= 0.643, \\ \lambda_8 &= 0.547. \end{aligned} \quad (29b)$$

To summarize, the basic model constants determined above are presented in Table 1.

The other useful constants which can be calculated using Table 1 and Eqs. (18d) and (23c) are listed in Table 2.

8. Comparison with Mellor–Yamada model and experimental data

a. Mellor–Yamada model

The MY model (Mellor and Yamada 1982) corresponds to

$$\begin{aligned} \lambda_1 &= 4 \left[6 \left(\frac{A_1}{B_1} \right)^2 + B_1^{-4/3} \right], \\ \lambda_2 &= \lambda_3 = \lambda_4 = \frac{1}{2} \lambda = \frac{3A_1}{B_1}, & \lambda_5 &= \frac{B_1}{3A_2}, \\ \lambda_6 &= \lambda_7 = 1, & \lambda_8 &= \frac{\tau_\theta}{\tau} = \frac{B_2}{B_1}. \end{aligned} \quad (30a)$$

Thus

$$\lambda = \frac{6A_1}{B_1}, \quad \alpha_1 = \alpha_2 = \alpha_3 = \gamma_1 = 0, \quad (30b)$$

where the constants A_1 , B_1 , A_2 and B_2 are determined by Mellor and Yamada to be

$$(A_1, B_1, A_2, B_2) = (0.92, 16.6, 0.74, 10.1), \quad (30c)$$

which correspond to a set of value for the model constants in the present model

$$\begin{aligned} (\lambda_1, \lambda_2, \lambda_3, \lambda_4) &= (0.168, 0.166, 0.166, 0.166) \\ (\lambda_5, \lambda_6, \lambda_7, \lambda_8, B_1) &= (7.48, 1, 1, 0.608, 16.6). \end{aligned} \quad (30d)$$

Substituting (30d) into (18d), (23c), and (24a) yields

$$Ri_c(\text{MY}) = 0.193. \quad (30e)$$

b. Comparison with measured data in neutral PBL

One of the deficiencies of the MY model, as Mellor and Yamada pointed out themselves, is that in a neutral boundary layer, the model cannot distinguish $\frac{1}{2}\overline{v^2}$ and $\frac{1}{2}\overline{w^2}$, the lateral and vertical components of the velocity variance, while experimental data consistently show that $\overline{w^2}$ is always significantly smaller than $\overline{v^2}$. Shir (1973) and Gibson and Launder (1978) added additional terms to the pressure correlations to parameterize the wall effects, assuming that in proximity to the wall, the transfer of turbulence energy from the horizontal to the vertical components is altered as the vertical extent of the eddies is suppressed. In this way $\overline{v^2}$ and $\overline{w^2}$ can accordingly be differentiated. The present model, however, offers an alternative that will be able to, at least partially, account for the difference between $\overline{v^2}$ and $\overline{w^2}$, without resorting

TABLE 1. Basic model constants.

λ_1	λ_2	λ_3	λ_4	λ_5	λ_6	λ_7	λ_8	B_1
0.107	0.0032	0.0864	0.1	11.04	0.786	0.643	0.547	19.3

to adding wall terms to the pressure correlations. In fact, the measured data indicate that the inequality of $\overline{v^2}$ and $\overline{w^2}$ may be mainly not due to the wall effects, as shown by Fig. 6 of Grant (1992), in which the ratio $\overline{w^2}/\overline{v^2}$ is roughly around 0.5, even far away from the boundaries; the ratio is never 1 at any height within the PBL. The present model employs the standard, advanced pressure correlations (without wall terms) into the model closure, which naturally allow $\overline{v^2}$ and $\overline{w^2}$ to be different. To see this we assume production equals dissipation in a neutral boundary layer, reducing (15a)–(15c) of the present model to

$$\frac{\overline{u^2}}{q^2} = \frac{1}{3} + \frac{\lambda_2 + 3\lambda_3}{3} \quad (31a)$$

$$\frac{\overline{v^2}}{q^2} = \frac{1}{3} - \frac{2\lambda_2}{3} \quad (31b)$$

$$\frac{\overline{w^2}}{q^2} = \frac{1}{3} + \frac{\lambda_2 - 3\lambda_3}{3}. \quad (31c)$$

In the MY model (and in all the second-closure PBL models known to us) $\lambda_2 = \lambda_3$, which makes $\overline{v^2} = \overline{w^2}$, while in the present model λ_2 and λ_3 are two independent parameters, and we choose to determine them according to Shih and Shabbir (1992)'s expressions that are derived from theoretical considerations. In Table 3 we compare the result of the present model in the neutral PBL with the measured data used by Mellor and Yamada (1982) and by Nieuwstadt (1985).

Since the difference between $\overline{v^2}$ and $\overline{w^2}$ is proportional to q^2 according to (31a)–(31c), and since q^2 typically decreases with height and nearly vanishes near the top of the PBL, $\overline{v^2} - \overline{w^2}$ also decreases and vanishes as height increases. Thus both the surface and the free flow cases are approximated.

The predicted value for $\overline{u^2}u_*^{-2}$ is smaller than the quoted data for the following reason: the quoted data were taken mostly in the lower part of the surface layer, while (31a)–(31c) give some weight to data in the middle and upper parts of the surface layer. The profiles of the measured data show that when the scaled height z/h (h is the PBL height) increases from the surface, $\overline{u^2}$ decreases

faster than $\overline{v^2}$ and $\overline{w^2}$ [see, e.g., Fig. 1a of Andr n (1991), in which $\overline{u^2}u_*^{-2}$ drops to below 3 at $z/h < 0.1$; Figs. 26 and 27 of Khurshudyan et al. (1981), in which while $\overline{u^2}$ decreases with height, $\overline{v^2}$ and $\overline{w^2}$ actually increase slightly for $z/h < 0.1$].

c. Comparison with measured and LES data in stratified flows

The turbulent Prandtl number, $\sigma_t = K_M/K_H$, is one of the important parameters of turbulence. We compare the inverse of σ_t as a function of the gradient Richardson number Ri resulting from both the present model and the MY model with the experimental data of Webster (1964). It is clear that turbulence in the stably stratified flow exists well beyond the MY critical value $Ri \approx 0.2$. According to the experimental data, the critical value of Ri should be of order unity, and the present model falls within the range of the measured data (Fig. 5).

We also compare the vertical and lateral heat flux ratio $-\overline{w\theta}/\overline{u\theta}$ (as a function of Ri resulting from both the present model and the MY model with the experimental data of Webster (1964). Webster described the ratio as “(being) seen to fall catastrophically from unity in neutral conditions to only about 0.5 at Ri equal to 0.2 and even less for higher Richardson numbers.” The present model gives the critical Richardson number $Ri_c = 0.96$, in agreement with the data (Fig. 6).

It is also informative to examine the nondimensional shear and potential temperature gradients defined as

$$\Phi_m = \frac{\kappa z}{u_*} S, \quad \Phi_h = -\frac{\kappa z u_*}{w\theta_s} \frac{\partial \Theta}{\partial z}, \quad (32)$$

where u_* and $\overline{w\theta_s}$ are the friction velocity and the surface potential temperature flux, respectively, and S is the shear given by Eq. (18b). Businger et al. (1971) analyzed the Kansas data in the constant flux surface layer and expressed Φ_m and Φ_h as functions of the dimensionless height ζ , which is the ratio between the height z and the Monin–Obukhov length L ,

TABLE 2. Derived constants. Useful constants calculated using Table 1 and Eqs. (18d) and (23c).

d_1	$7.0682 \cdot 10^{-2}$	s_0	$5.3500 \cdot 10^{-2}$	c_1	$1.6634 \cdot 10^{-3}$
d_2	$7.0424 \cdot 10^{-3}$	s_1	$2.3779 \cdot 10^{-3}$	c_2	$1.6148 \cdot 10^{-3}$
d_3	$5.5819 \cdot 10^{-4}$	s_2	$-2.2425 \cdot 10^{-5}$	c_3	$1.6170 \cdot 10^{-5}$
d_4	$3.4731 \cdot 10^{-4}$	s_4	$6.0386 \cdot 10^{-2}$	c_4	$2.0175 \cdot 10^{-1}$
d_5	$-3.1275 \cdot 10^{-6}$	s_5	$5.4698 \cdot 10^{-4}$	c_5	$-3.9415 \cdot 10^{-2}$
		s_6	$6.8435 \cdot 10^{-5}$		

TABLE 3. Measured data and present model prediction in neutral PBL.

Data/Model	$\overline{u^2}/u_*^2$	$\overline{v^2}/u_*^2$	$\overline{w^2}/u_*^2$	B_1
Data (MY)	3.61	1.74	1.15	16.6
Data (Nieuwstadt)	4.2	3	1.9	27.4
Present model prediction	3.03	2.38	1.78	19.3

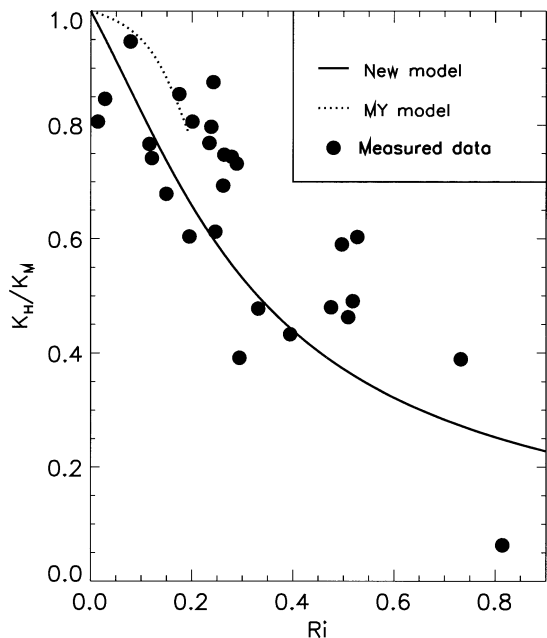


FIG. 5. The inverse turbulent Prandtl number σ_T^{-1} (normalized by its value for neutral stratification) vs the gradient Richardson number. The solid line is the result of the present model at level 2. The dotted line represents the level-2 MY model. The experimental data by Webster (1964) are redrawn here as filled circles. The present model yields a much larger critical Richardson number (≈ 1) than the Mellor–Yamada model (≈ 0.2).

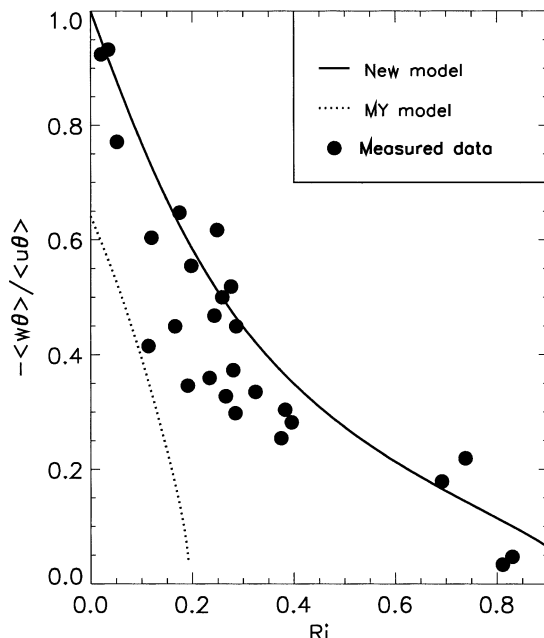


FIG. 6. Ratio of the rates of heat transport in the w direction (vertical) and the u direction (horizontal, along the mean flow), $-\langle w\theta \rangle / \langle u\theta \rangle$, vs the Richardson number. The solid line represents the result of the present model, while the dotted line represents the MY model. The experimental data (Webster 1964) are redrawn here as filled circles.

$$\Phi_m = \begin{cases} (1 - 15\zeta)^{-1/4}: & \zeta < 0 \\ 1 + 4.7\zeta: & \zeta > 0 \end{cases} \quad (33a)$$

$$\Phi_h = \begin{cases} 0.74(1 - 9\zeta)^{-1/2}: & \zeta < 0 \\ 0.74 + 4.7\zeta: & \zeta > 0, \end{cases} \quad (33b)$$

where

$$\zeta \equiv \frac{z}{L}, \quad L \equiv \frac{-\Theta u_*^3}{\kappa g w \theta}. \quad (33c)$$

In deriving (33a–b) Businger et al. assumed $\kappa = 0.35$, where κ is the von Kármán’s constant. Höögström (1988) subsequently modified Businger et al.’s formula with the more commonly accepted values for von Kármán’s constant $\kappa = 0.4$ and for Φ_h at neutrality, $(\Phi_h)_{\zeta=0} = 0.95$:

$$\Phi_m = \begin{cases} (1 - 19.3\zeta)^{-1/4}: & \zeta < 0 \\ 1 + 6\zeta: & \zeta > 0 \end{cases} \quad (34a)$$

$$\Phi_h = \begin{cases} 0.95(1 - 11.6\zeta)^{-1/2}: & \zeta < 0 \\ 0.95 + 7.8\zeta: & \zeta > 0. \end{cases} \quad (34b)$$

The MY model (Mellor 1973; Mellor and Yamada 1982), by assuming $\ell = \kappa z$ in the surface layer, matches the original Businger et al.’s formula very well except for Φ_m in the unstable region ($\zeta < 0$), where the MY model underestimates the Kansas data by about 50%.

Recently Nakanishi (2001) has shown that in the surface layer, as indicated by the LES data, ℓ depends on ζ as follows:

$$l = \begin{cases} \kappa z: & \zeta < 0 \\ \kappa z(1 + 2.7\zeta)^{-1}: & \zeta > 0. \end{cases} \quad (35)$$

In the present level-2 model, the expressions for Φ_m and Φ_h in terms of ζ (via Ri) as well as $\ell/(\kappa z)$ are as follows:

$$\Phi_m(\text{Ri}) = \frac{\sqrt{2}G_M^{1/4}(\text{Ri})}{B_1 S_M^{1/2}(\text{Ri})} \left(\frac{l}{\kappa z} \right)^{-1},$$

$$\Phi_h(\text{Ri}) = \frac{\Phi_m(\text{Ri})S_M(\text{Ri})}{S_H(\text{Ri})}, \quad \zeta(\text{Ri}) = \frac{\text{Ri}\Phi_m^2(\text{Ri})}{\Phi_h(\text{Ri})}. \quad (36)$$

Using Eqs. (35)–(36), we plot in Figs. 7 and 8 Φ_m and Φ_h versus ζ for both unstable and stable conditions, and compare them with the Kansas data as originally formulated by Businger et al. (1971) and as modified by Höögström (1988). We also plot the results of the MY model using the length scale (35). The comparison shows that:

- 1) In the unstable region ($\zeta < 0$), the present model (solid line) improves significantly the MY model (dotted line) for Φ_m , and improves Φ_h slightly.
- 2) In the stable region ($\zeta > 0$), both the present model and the MY model fall within the (scattered) data

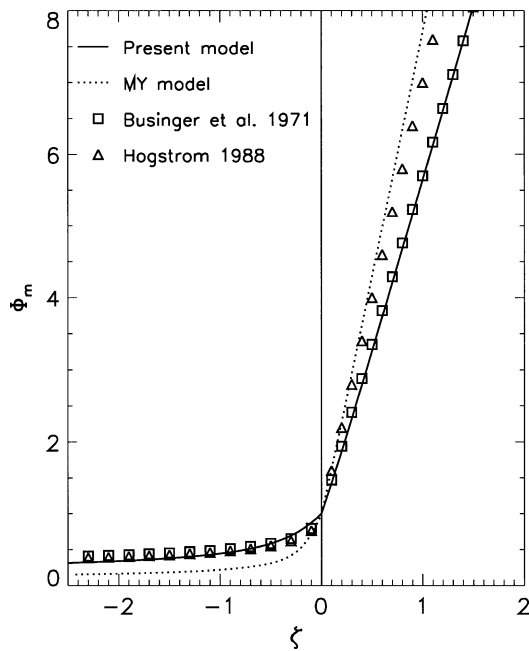


FIG. 7. The nondimensional shear Φ_m as a function of $\zeta = z/L$. The solid line represents the results using the present model, while the dotted line corresponds to the MY model. The squares represent the Kansas data formulated by Businger et al. (1971), while the triangles represent Businger et al.'s formula modified by Höögström (1988).

regions. For more stable cases, however, the two models will further diverge, as we will show below.

In recent years, several LESs have provided Φ_m^{-1} and Φ_h^{-1} as functions of the gradient Richardson number Ri (e.g., Mason 1994; Brown et al. 1994; Andrén 1995; Kosovic and Curry 2000). The Wangara data have also been analyzed and the resulting Φ_m^{-1} and Φ_h^{-1} plotted (Carson and Richards 1978). In all these studies, turbulence exists with significant intensity around the commonly accepted value of the critical Richardson number 0.2, and extends up to Ri of order unity. Since the most recent LES by Kosovic and Curry (2000) use a more advanced subgrid model, we choose to compare with their results. We employ both the present model and the MY model to simulate the same stably stratified PBL used by Kosovic and Curry (2000), and compare the models results with their LES of the high-resolution case NLHRB, at hour 12, when a quasi-steady state is reached.

In our simulation, we use the level-2 model since we are particularly interested in the behavior of the model when the gradient Richardson number Ri varies. While the level-2.5 and -3 models depend on two independent parameters, G_M and G_H , the level-2 model depends on only one parameter, Ri . In the PBL we chose to simulate, the diffusion terms are very small (see Fig. 11 of Kosovic and Curry 2000). We have also run the level-2.5

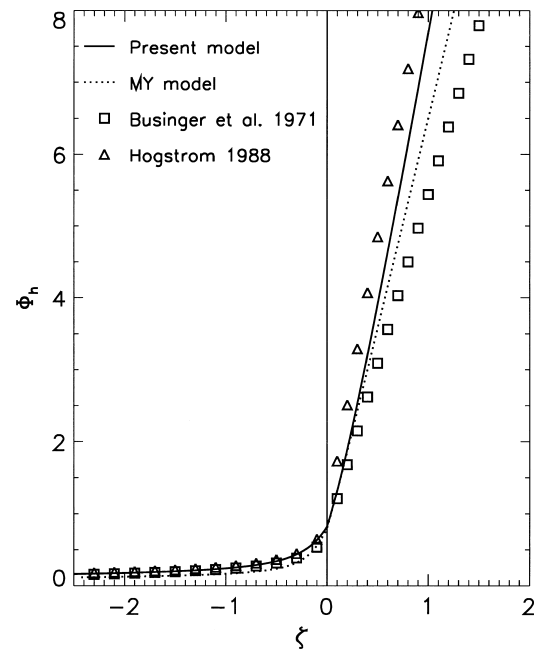


FIG. 8. Same as Fig. 7 but for the nondimensional potential temperature gradient Φ_h .

and -3 models using the usual downgradient approximations for the diffusion terms, and the results are very close to those from the level-2 model.

In fact, to see the full benefits of level-2.5 and -3 models, one needs to parameterize the third moments much better than by the downgradient approximation. As stated in the introduction, in the present study we concentrate on the improvements due to the new pressure correlation parameterizations, and leave the third moment parameterizations for future study. Thus the level-2 model with a commonly used length scale formula, Eq. (5e), is most appropriate for testing the model.

In Figs. 9 and 10 we plot Φ_m^{-1} and Φ_h^{-1} as functions of Ri . The graphs indicate that, in the context of Monin–Obukhov similarity theory, for $Ri < 0.2$, the present model recovers the observed Kansas data as analyzed by Businger et al. (1971) and modified by Höögström (1988). For $Ri > 0.2$, the present model still produces significant turbulence, in agreement with the LES data by Kosovic and Curry (2000), which is consistent with the LES of Mason (1994), Brown et al. (1994), and Andrén (1995) and the Wangara data analyzed by Carson and Richards (1978). In the figures we also plot the results of the MY model, which fail to reproduce the turbulence beyond $Ri = 0.2$ found in the LES.

The differences between the present model and the LES results are probably due to the neglect of the diffusion terms and the imperfect parameterization of the turbulence length scale, and search for better parameterizations of these two crucial components of the closure modeling should be among the subjects of future studies.

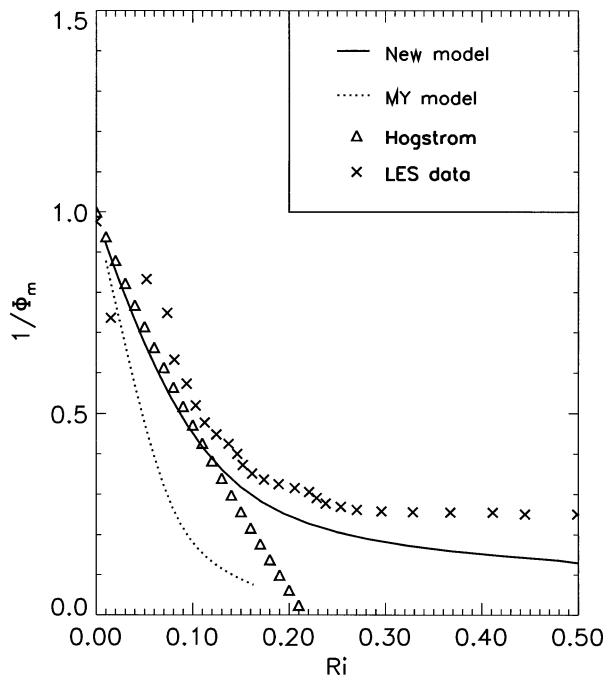


FIG. 9. The reciprocal of the nondimensional shear, Φ_m^{-1} , as a function of the gradient Richardson number. The crosses represent the LES simulation of Kosovic and Curry (2000), case NLHRB, at hour 12. The solid line represents simulation results using the present model, while the dotted line, simulation results using the MY model. The triangles represent the Kansas data formulated by Businger et al. (1971) and modified by Höögström (1988).

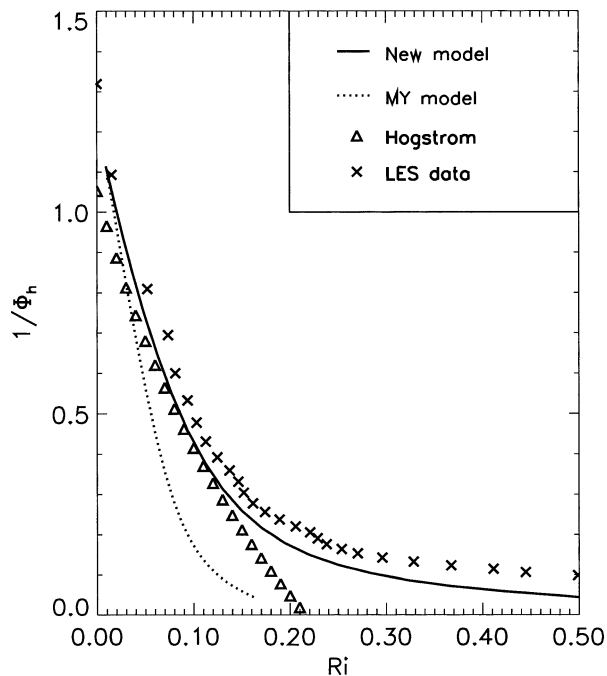


FIG. 10. Similar to Fig. 9 but for the reciprocal of the nondimensional potential temperature gradient, Φ_h^{-1} .

The PBL height is one of the most important quantities in any PBL modeling. The PBL height is usually defined as the height at which the turbulent kinetic energy or the magnitude of the momentum flux decreases to a small fraction of the corresponding surface value; or it may be defined as the height at which the (positive) temperature gradient reaches a certain value from below. In any case, the top of the PBL lies in a region where the turbulence is stably stratified and, given the mean profiles of the wind and the temperature (and thus given Ri), a higher intensity level of turbulence yields a greater PBL height. The MY model, however, underestimates the PBL height (Yamada and Mellor 1975). Since the present model predicts larger critical Richardson number and produces more turbulence for a given Richardson number, greater PBL heights can be achieved (Fig. 11).

9. Conclusions

With the application of the updated expressions for the pressure–velocity and pressure–temperature correlations and the use of the turbulence timescale ratios fixed by recent RNG, we have derived a second-order closure turbulence model to describe the PBL.

One of the improvements brought about by the present model is that it distinguishes the vertical and the

lateral components of the turbulence kinetic energy in neutral PBLs without the complexity of the wall functions, something that was not achieved by previous second-order closure PBL models.

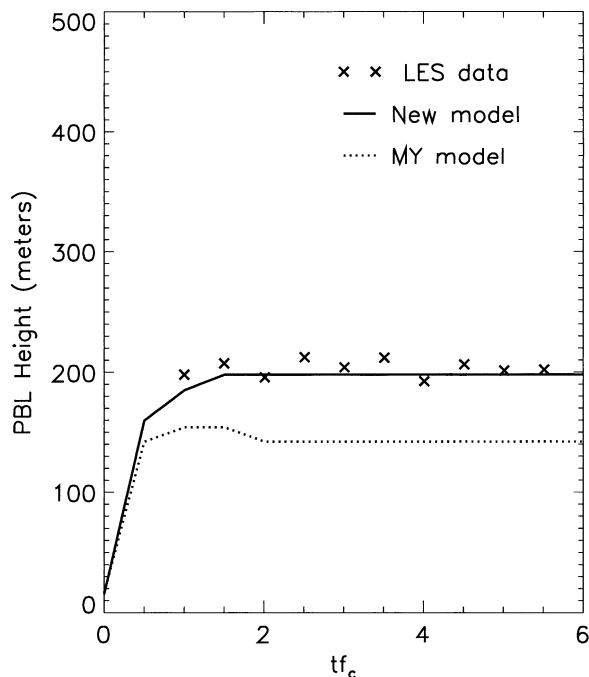


FIG. 11. PBL height as a function of the dimensionless time tf_c , where f_c is the Coriolis parameter. Cross: LES result; solid line: present model result; dotted line: MY model result.

A main feature of the new model is that it yields a critical Richardson number (Ri_c) of order unity, rather than ~ 0.2 , as given by most previous models. The larger critical Richardson number is in agreement with measured and LES data and the stability analysis that includes nonlinear interactions. The new model compares better than the previous models with the Kansas data as analyzed by Businger et al. (1971) and modified by Högström (1988) for both the unstable case ($Ri < 0$) and the stable case when $Ri < 0.2$. While most previous models predict no turbulence for $Ri > 0.2$, the present model reproduces closely the LES and laboratory data for Richardson numbers up to order unity.

In addition, the new model produces greater PBL height than the previous models.

Acknowledgments. The authors thank Drs. B. Kosovic and J.A. Curry for providing their LES data to be used in this paper.

APPENDIX

The Level-3 PBL Model

In the level-3 PBL model, the turbulent temperature variance $\overline{\theta^2}$ is solved from its prognostic equation [which replaces the algebraic equation (14)]:

$$\frac{D}{Dt} \overline{\theta^2} + \frac{\partial}{\partial z} \overline{w\theta^2} = -2 \frac{\partial \Theta}{\partial z} \overline{w\theta} - 2 \frac{\overline{\theta^2}}{\tau_\theta}. \quad (A1)$$

From (10a)–(10b), the algebraic equation for the heat flux $\overline{w\theta}$ is

$$\begin{aligned} \overline{w\theta} = & -\lambda_5^{-1} \tau \left[\frac{\partial \Theta}{\partial z} \overline{w^2} + \frac{1}{2} (\lambda_6 - \lambda_7) \left(\frac{\partial U}{\partial z} \overline{u\theta} + \frac{\partial V}{\partial z} \overline{v\theta} \right) \right] \\ & + \lambda_5^{-1} \lambda_0 g \alpha \tau \overline{\theta^2}. \end{aligned} \quad (A2)$$

All the other algebraic equations for the Reynolds stress and the heat flux, except (15i), which is replaced by (A2), are the same as the level-2.5 model (15a)–(15h). We solve (15a)–(15h) and (A2) using symbolic algebra and the results are

$$\begin{aligned} (\overline{uw}, \overline{vw}) &= -e\tau S_M \left(\frac{\partial U}{\partial z}, \frac{\partial V}{\partial z} \right), \\ \overline{w\theta} &= -e\tau S'_H \frac{\partial \Theta}{\partial z} + \gamma_c, \end{aligned} \quad (A3)$$

where

$$\gamma_c = \frac{\lambda_5^{-1} \left[1 + \lambda_4 \lambda_5^{-1} G_H + \left(\lambda_3^2 - \frac{1}{3} \lambda_2^2 \right) G_M \right]}{D} \lambda_0 g \alpha \tau \overline{\theta^2} \quad (A4)$$

is the countergradient term, which is absent in the level-2.5 model and D is of the same form as in (18c). The

structure of the stability function S_M differs from the S_M in the level-2.5 model (17a) by an extra term,

$$S_M = \frac{1}{D} \left[s_0 + s_1 G_H + s_2 G_M + s_3 (g\alpha\tau)^2 \frac{\overline{\theta^2}}{e} \right], \quad (A5)$$

where

$$\begin{aligned} s_3 &= \lambda_0 \lambda_4 \lambda_5^{-1} \left[\lambda_3 + \frac{1}{3} \lambda_2 + \frac{1}{2} \lambda_5^{-1} (\lambda_6 + \lambda_7) \right] \\ \lambda_0 &= 1 - \gamma_1 = \frac{2}{3} \end{aligned} \quad (A6)$$

λ_0 is a new model constant in the level-3 model, and s_3 is a new derived constant. Note that in (A3) we use S'_H instead of S_H for the stability function because of the existence of the countergradient term γ_c . The form of the function S'_H is the same as S_H in the level-2.5 model (17b). The model constants B_1 and λ 's are the same as in Table 1 except that now $\lambda_8 = 0$. The expressions for the derived constants d 's and s 's are the same as in (18d) with $\lambda_8 = 0$.

REFERENCES

- Abarbanel, H. D., D. D. Holm, J. E. Marsden, and T. Ratiu, 1984: Richardson number criterion for the non-linear stability of 3D stratified flow. *Phys. Res. Lett.*, **52**, 2352–2355.
- André, J. C., G. DeMoor, P. Lacarrère, G. Thery, and R. du Vachat, 1978: Modeling the 24 h evolution of the mean and turbulent structures of the planetary boundary layer. *J. Atmos. Sci.*, **35**, 1861–1883.
- Andrén, A., 1991: A TKE-dissipation model for the atmospheric boundary layer. *Bound.-Layer Meteor.*, **56**, 207–221.
- , 1995: The structure of stably stratified atmospheric boundary layers: A large-eddy simulation study. *Quart. J. Roy. Meteor. Soc.*, **121**, 961–985.
- , and C.-H. Moeng, 1993: Single-point closures in a neutrally stratified boundary layer. *J. Atmos. Sci.*, **50**, 3366–3379.
- Batchelor, G. K., 1971: *The Theory of Homogeneous Turbulence*. 2d ed. Cambridge University Press, 197 pp.
- Blackadar, A. K., 1962: The vertical distribution of wind and turbulent exchange in neutral atmosphere. *J. Geophys. Res.*, **67**, 3095–3102.
- Brown, A. R., S. H. Derbyshire, and P. J. Mason, 1994: Large-eddy simulation of stable atmospheric boundary layers with a revised stochastic subgrid model. *Quart. J. Roy. Meteor. Soc.*, **120**, 1485–1512.
- Businger, J. A., J. C. Wyngaard, Y. Izumi, and E. F. Bradley, 1971: Flux-profile relationships in the atmospheric surface layer. *J. Atmos. Sci.*, **28**, 181–189.
- Canuto, V. M., 1994: Large eddy simulation of turbulence: A subgrid model including shear, vorticity, rotation and buoyancy. *Astrophys. J.*, **428**, 729–752.
- , and M. S. Dubovikov, 1996a: A dynamical model for turbulence. I. General formalism. *Phys. Fluids*, **8**, 571–586.
- , and —, 1996b: A dynamical model for turbulence. II. Shear-driven flows. *Phys. Fluids*, **8**, 587–598.
- , and —, 1997: A dynamical model for turbulence. IV. Buoyancy driven flows. *Phys. Fluids*, **9**, 2118–2131.
- , F. Minotti, C. Ronchi, R. M. Ypma, and O. Zeman, 1994: Second-order closure PBL model with new third-order moments: Comparison with LES data. *J. Atmos. Sci.*, **51**, 1605–1618.
- , Y. Cheng, and A. Howard, 2001: New third-order moments for the convective boundary layer. *J. Atmos. Sci.*, **58**, 1169–1172.

- Carson, D. J., and P. J. R. Richards, 1978: Modeling surface turbulent fluxes in stable conditions. *Bound.-Layer Meteor.*, **14**, 67–81.
- Cheng, Y., and V. M. Canuto, 1994: Stably stratified shear turbulence: A new model for the energy dissipation length scale. *J. Atmos. Sci.*, **51**, 2384–2396.
- Chou, P. Y., 1940: On an extension of Reynolds' method of finding apparent stress and the nature of turbulence. *Chinese J. Phys.*, **4**, 1–33.
- , 1945: On velocity correlations and the solutions of the equations of turbulent fluctuation. *Quart. Appl. Math.*, **3**, 38–54.
- D'Alessio, S. J. D., K. Abdella, and N. A. McFarlane, 1998: A new second-order turbulence scheme for modeling the ocean mixed layer. *J. Phys. Oceanogr.*, **28**, 1624–1641.
- Deardorff, J. W., 1980: Stratocumulus-capped mixed layers derived from a three-dimensional model. *Bound.-Layer Meteor.*, **18**, 495–527.
- Enger, L., 1986: A higher order closure model applied to dispersion in a convective PBL. *Atmos. Environ.*, **20**, 879–894.
- Galperin, B., L. H. Kantha, S. Hassid, and A. Rosati, 1988: A quasi-equilibrium turbulent energy model for geophysical flows. *J. Atmos. Sci.*, **45**, 55–62.
- Gambo, K., 1978: Notes on the turbulent closure model for atmospheric boundary layers. *J. Meteor. Soc. Japan*, **56**, 466–480.
- Gerz, T., U. Schumann, and S. E. Elghobashi, 1989: Direct numerical simulation of stratified, homogeneous turbulent shear flows. *J. Fluid Mech.*, **220**, 563–594.
- Gibson, M. M., and B. E. Launder, 1978: Ground effects on pressure fluctuations in the atmospheric boundary layer. *J. Fluid Mech.*, **86**, 491–511.
- Grant, A. L. M., 1992: The structure of turbulence in the near-neutral atmospheric boundary layer. *J. Atmos. Sci.*, **49**, 226–239.
- Hassid, S., and B. Galperin, 1983: A turbulent energy model for geophysical flows. *Bound.-Layer Meteor.*, **26**, 397–412.
- Högström, U., 1988: Non-dimensional wind and temperature profiles in the atmospheric surface layer: A re-evaluation. *Bound.-Layer Meteor.*, **42**, 55–78.
- Howard, L. N., 1961: Note on a paper by J. W. Miles. *J. Fluid Mech.*, **10**, 509–512.
- Kaimal, J. C., J. C. Wyngaard, Y. Izumi, and O. R. Coté, 1972: Spectral characteristics of surface layer turbulence. *Quart. J. Roy. Meteor. Soc.*, **98**, 563–589.
- Kantha, L. H., and C. A. Clayson, 1994: An improved mixed layer model for geophysical applications. *J. Geophys. Res.*, **99** (C12), 25 235–25 266.
- Khurshudyan, L. H., W. H. Snyder, and I. V. Nekrasov, 1981: Flow and dispersion of pollutant over two-dimensional hills: Summary report on joint Soviet–American study. Environmental Protection Agency document EPA 600/4-81-067, 130 pp.
- Kosovic, B., and J. A. Curry, 2000: A large eddy simulation of a quasi-steady, stably stratified atmospheric boundary layer. *J. Atmos. Sci.*, **57**, 1052–1068.
- Launder, B. E., G. Reece, and W. Rodi, 1975: Progress in the development of a Reynolds-stress turbulent closure. *J. Fluid Mech.*, **68**, 537–566.
- Lumley, J. L., 1978: Computational modeling of turbulent flows. *Adv. Appl. Mech.*, **18**, 123–176.
- , and B. Khajeh-Nouri, 1974: Computational modeling of turbulent transport. *Advances in Geophysics*, Vol. 18A, Academic Press, 169–192.
- Martin, P. J., 1985: Simulation of the mixed layer at OWS November and Papa with several models. *J. Geophys. Res.*, **90**, 903–916.
- Mason, P. J., 1994: Large-eddy simulation: A critical review of the technique. *Quart. J. Roy. Meteor. Soc.*, **120**, 1–26.
- Mellor, G. L., 1973: Analytic prediction of the properties of stratified planetary surface layers. *J. Atmos. Sci.*, **30**, 1061–1069.
- , and T. Yamada, 1974: A hierarchy of turbulence closure models for planetary boundary layer. *J. Atmos. Sci.*, **31**, 1791–1806.
- , and —, 1982: Development of a turbulence closure model for geophysical fluid problems. *Rev. Geophys. Space Phys.*, **20**, 851–875.
- Miles, J. W., 1961: On the stability of heterogeneous shear flows. *J. Fluid Mech.*, **10**, 496–508.
- Moeng, C.-H., and J. C. Wyngaard, 1986: An analysis of closures for pressure-scalar covariances in the convective boundary layer. *J. Atmos. Sci.*, **43**, 2499–2513.
- , and —, 1989: Evaluation of turbulent transport and dissipation closures in second-order modeling. *J. Atmos. Sci.*, **46**, 2311–2330.
- , and P. P. Sullivan, 1994: A comparison of shear- and buoyancy-driven planetary boundary layer flows. *J. Atmos. Sci.*, **51**, 999–1022.
- Monin, A. S., and A. M. Yaglom, 1971: *Statistical Fluid Mechanics*. Vols. 1, 2, The MIT Press, 874 pp.
- Nakanishi, M., 2001: Improvement of the Mellor–Yamada turbulence closure model based on large-eddy simulation data. *Bound.-Layer Meteor.*, **99**, 349–378.
- Nieuwstadt, F. T. M., 1985: A model for the stationary, stable boundary layer. *Turbulence and Diffusion in Stable Environments*, J. C. R. Hunt, Ed., Clarendon Press, 149–179.
- Pope, S. B., 1975: A more general effective viscosity hypothesis. *J. Fluid Mech.*, **72**, 331–340.
- Rotta, J. C., 1951: Statistische theorie nichthomogener Turbulenz. *Z. Phys.*, **129**, 547–572.
- Shih, T.-H., and A. Shabbir, 1992: Advances in modeling the pressure correlation terms in the second moment equations. *Studies in Turbulence*, T. B. Gatski, S. Sarkar, and C. G. Speziale, Eds., 91–128.
- Shir, C. C., 1973: A preliminary numerical study of atmospheric turbulent flows in the idealized planetary boundary layer. *J. Atmos. Sci.*, **30**, 1327–1339.
- Speziale, C. G., 1991: Analytical methods for the development of Reynolds-stress closures in turbulence. *Annu. Rev. Fluid Mech.*, **23**, 107–157.
- Strang, E. J., and H. J. S. Fernando, 2001: Vertical mixing and transports through a stratified shear layer. *J. Phys. Oceanogr.*, **31**, 2026–2048.
- Therry, G., and P. Lacarrère, 1983: Improving the eddy kinetic energy model for planetary boundary layer description. *Bound.-Layer Meteor.*, **25**, 63–88.
- Wang, D., W. G. Large, and J. C. McWilliams, 1996: Large-eddy simulation of the equatorial ocean boundary layer: Diurnal cycling, eddy viscosity, and horizontal rotation. *J. Geophys. Res.*, **101**, 3649–3662.
- Webster, C. A. G., 1964: An experimental study of turbulence in a density stratified shear flow. *J. Fluid Mech.*, **19**, 221–245.
- Wichmann, M., and E. Schaller, 1986: On the determination of the closure parameters in higher-order closure models. *Bound.-Layer Meteor.*, **37**, 323–341.
- Yamada, N., 1985: Model for the pressure terms in the equations for second-order turbulent moment, and its application to the atmospheric surface layer. *J. Meteor. Soc. Japan*, **63**, 695–701.
- Yamada, T., and G. Mellor, 1975: A simulation of the Wangara boundary layer data. *J. Atmos. Sci.*, **32**, 2309–2329.
- Young, S. T. B., 1975: Turbulence measurements in a stably-stratified turbulent shear flow. Queen Mary College of London Rep. QMC-EP 6018.
- Zeman, O., and J. L. Lumley, 1979: Buoyancy effects in entraining turbulent boundary layers: A second-order closure study. *Turbulent Shear Flows*, Vol. 1, F. Durst et al. Eds., Berlin, 295–302.